

Solution of Nonlinear Polarization Boundary Conditions

E. Chisholm, L. J. Gray and G. E. Giles
Oak Ridge National Laboratory
Oak Ridge, Tennessee 37831-6367 U.S.A.

Abstract

An efficient algorithm for solving multiple reaction electrochemical polarization equations is presented. The boundary integral formulation for the electric field (Laplace equation) conveniently provides a direct relationship between potential and current at the electrode surfaces, which can then be coupled to the nonlinear polarization boundary conditions. As a consequence, a successful Gauss-Seidel type iteration, incorporating a nonlinear solve at each step, can be developed. Results are presented for the modeling multiple chemical reactions in an electrospray emitter tube.

1 Introduction

Boundary integral equation methods [1, 2] have been used very successfully to solve a number of industrial and scientific problems involving electrochemical reactions [3, 4]. These include the modeling and design of cathode protection systems (see [5, 6, 7, 8] and references therein), modeling of industrial electroforming operations [9, 10, 11], simulation of Scanning Electrochemical Microscopy [12, 13, 14, 15] and, of particular interest herein, the analysis of an electrospray emitter tube [16, 17]. This emitter tube converts material in solution to gas phase ions that can be analyzed by a mass spectrometer.

For electrochemical problems in general, the interest is in surface quantities, and in particular, the surface current density. The integral equation formulation of the governing Laplace equation provides this surface solution (without a volume discretization) and, moreover, the current is computed directly, *i.e.*, without a numerical differentiation of the potential function. Direct solution of the surface current is particularly important, in that electrochemistry applications generally involve nonlinear *polarization* boundary conditions [18, 19]. That is, the boundary conditions on the anode and cathode are not simply the applied voltages, but instead the surface potential and current must satisfy a complicated relationship (which may only be available as an experimentally determined voltage/current curve). These polarization equations represent the details of the electrochemical reactions occurring near the electrode surfaces. In general, the direct relationship between surface potential and current provided by the boundary integral equation yields a more accurate solution for the current, clearly beneficial in solving the polarization equations. Equally important, a boundary integral analysis allows the nonlinear algorithm to work solely with the surface quantities, rather than having to contend with convergence of the volume solution in the course of the iteration.

Nevertheless, solving the polarization equations can, for a number of reasons, be quite challenging. In the first place, although the polarization is ‘local’ (point by point), all polarization values are very much coupled through the solution of the Laplace equation. Depending upon the geometry of the problem, this can be a very large coupled system, making each iteration computationally expensive. Second, depending upon the parameters of the system, the voltage/current relationship can be highly nonlinear. Finally, as in the electrospray analysis considered herein, multiple electrochemical reactions can be taking place, and these reactions are not independent. This coupling further complicates the equations, thus making convergence to a solution more difficult. The work reported herein was motivated by the failure of simple nonlinear algorithms to converge quickly, or at all, for polarization equations arising in electrospray simulations.

In this paper, the boundary integral formulation of the Laplace equation is exploited to develop a new efficient algorithm for solving nonlinear polarization boundary conditions, with the emphasis on difficult *multiple reaction* models. It is applied to single and dual reactions occurring in electrospray emitter tubes, but it is expected that this technique will be effective for other electrochemical simulations. The next section briefly describes preliminary material, the governing electrochemical equations and the boundary integral analysis. Section 3 indicates that a simple approach to solving the polarization is entirely inadequate, and the new algorithm is presented in Section 4. Numerical results using this approach are described in Section 5.

2 Governing Equations

The physical system (the electrochemical ‘cell’) that this analysis models consists of an electrolyte volume bounded by a combination of insulated surfaces, one anode and one cathode. A potential difference (cell voltage) is applied across the anode and cathode, creating a potential distribution and a current field inside the electrolyte volume. In the electrolyte it is assumed that the electric field is obtained from a potential function ϕ , and that this function satisfies the Laplace equation

$$\nabla^2\phi = \left(\frac{\partial^2}{\partial x^2} + \frac{\partial^2}{\partial y^2} + \frac{\partial^2}{\partial z^2} \right) \phi = 0 . \quad (1)$$

The electric field is the gradient of ϕ , $\mathbf{E} = -\nabla\phi$, and the current density $\mathcal{I}(P)$ at a surface point $P = (x_P, y_P, z_P)$ is

$$\mathcal{I} = \kappa\mathbf{E} \cdot \mathbf{n} = -\kappa \frac{\partial\phi}{\partial n} . \quad (2)$$

Here κ is the electrolyte conductivity, and \mathbf{n} is the unit outward normal at P .

In general, obtaining a unique solution of Eq. (1) requires that either the potential or current be known at each point on the boundary. In electrochemistry applications however, the specified boundary data on the electroactive surfaces

(anode, cathode) are replaced by polarization equations which relate surface potential and surface current. In the electrospray application presented below, the cathode is a ‘virtual’ cathode (meaning an isopotential surface with no electrochemical reactions), and thus polarization is only present on the anode surface. The following discussion therefore only considers the anode, it being understood that a real cathode could be treated similarly. In addition, for simplicity, this section only presents the equations for a single reaction. The equations for coupling multiple simultaneous reactions have been described in [17], and will be briefly reviewed in Section 4.2.

The cell voltage is composed of the sum of the anode and cathode interfacial potential differences (IPD) and the IR voltage drop in the electrolyte. For this system with a virtual cathode, there is no cathode IPD. Due to electrochemical reactions at the anode surface, the potential $\phi_A(Q)$ at the electrolyte boundary is given by

$$\phi_A(Q) = \phi_0 + \eta_A(Q) \quad (3)$$

where ϕ_0 is the applied potential on the anode, $\eta_A(Q)$ is the polarization (collectively, the IPD), and Q is a point on the anode. To simplify notation, the Q will be dropped, it being understood that the polarization as defined here varies over the anode surface. In this work we assume that, for each reaction, the polarization is composed of three components

$$\eta_A = \eta_E + \eta_{act} + \eta_{con} . \quad (4)$$

The equilibrium potential η_E is a constant with respect to a reference half-cell potential such as H_2/H^+ ; it depends upon the particular reaction, and is the minimum potential necessary for the reaction to proceed. The activation and concentration polarizations for this reaction, η_{act} and η_{con} respectively, are functions of the local current. The activation polarization is related to the current through the Butler-Volmer equation [18, 19]

$$\mathcal{I} = \mathcal{I}_0 \left(e^{\frac{\alpha_A F}{RT} \eta_{act}} - e^{-\frac{\alpha_C F}{RT} \eta_{act}} \right), \quad (5)$$

where F is Faraday’s constant, R is the gas constant, and T is the temperature in Kelvin. The reaction dependent parameters are the exchange current \mathcal{I}_0 , and the transfer coefficients α_A and α_C . The concentration polarization [18, 19] depends upon two additional parameters, the ion valence n_v and the limiting current \mathcal{I}_L via

$$\eta_{con} = \frac{RT}{n_v F} \log \left(1 - \frac{\mathcal{I}}{\mathcal{I}_L} \right). \quad (6)$$

The simultaneous solution of Eqs. 1 and 3, together with the remaining boundary conditions, is therefore a coupled system of nonlinear equations, and an efficient algorithm for solving this system is the subject of this paper.

2.1 Boundary Integral Formulation

The boundary integral equation for the Laplace equation $\nabla^2\phi = 0$ is usually written in terms of the potential ϕ and flux $\partial\phi/\partial n$. For electrochemistry applications it is convenient to replace the flux with the current density Eq. (2). This integral equation then takes the form [2, 20]

$$\mathcal{P}(P) \equiv \phi(P) + \int_{\Sigma} \phi(Q) \frac{\partial G}{\partial \mathbf{n}}(P, Q) dQ + \frac{1}{\kappa} \int_{\Sigma} G(P, Q) \mathcal{I}(Q) dQ = 0 . \quad (7)$$

Here $\mathbf{n} = \mathbf{n}(Q)$, denotes the unit outward normal on the boundary surface Σ , and P and Q points on Σ . In three dimensions, the fundamental solution (Green's function) $G(P, Q)$ is usually taken as the point source potential

$$G(P, Q) = \frac{1}{4\pi r} , \quad (8)$$

where $R = Q - P$ and $r = \|R\|$ is the distance between P and Q . In general, Eq. (7) is reduced to a finite system of linear equations by approximating the surface Σ in terms of elements defined by M nodal points, and then interpolating the surface potential and flux in terms of the values at these nodes. This results in a matrix system

$$H [\phi] = G [\mathcal{I}] \quad (9)$$

where H and G are $M \times M$ matrices, and $[\phi]$ and $[\mathcal{I}]$ are column vectors of the nodal values of potential and current. Taking into account the known boundary conditions, these equations must be solved simultaneously with the polarization equations on the anode, Eq. (3). In this work, the matrices H and G are obtained from the boundary integral equation by means of a Galerkin approximation [20]. A quadratic interpolation of the surface (six-noded triangles) and the boundary functions is employed. Thus, for an element defined by nodal points $\{Q_j = (x_j, y_j, z_j)\}$, $1 \leq j \leq 3$ for the vertices, $4 \leq j \leq 6$ for the mid-side nodes, the interpolation of the boundary surface and boundary potential are given by

$$\begin{aligned} \Sigma(\eta, \xi) &= \sum_{j=1}^6 (x_j, y_j, z_j) \psi_j(\eta, \xi) \\ \phi(\eta, \xi) &= \sum_{j=1}^6 \phi(Q_j) \psi_j(\eta, \xi) . \end{aligned} \quad (10)$$

The shape functions ψ_j are

$$\begin{aligned} \psi_1(\eta, \xi) &= (1 - \eta - \xi)(1 - 2\eta - 2\xi) & \psi_4(\eta, \xi) &= 4\eta(1 - \eta - \xi) \\ \psi_2(\eta, \xi) &= \eta(2\eta - 1) & \psi_5(\eta, \xi) &= 4\eta\xi \\ \psi_3(\eta, \xi) &= \xi(2\xi - 1) & \psi_6(\eta, \xi) &= 4\xi(1 - \eta - \xi) \end{aligned} \quad (11)$$

where the parameter space is the right triangle $0 \leq \eta \leq 1$, $0 \leq \xi \leq 1$, and $0 \leq \eta + \xi \leq 1$.

3 Simple nonlinear algorithm

As motivation for the development of a new solution algorithm, we first describe the failure of a simple direct method. The simplest, admittedly too naive, approach to solving the coupled nonlinear equations is what is termed a ‘Picard iteration’, or more descriptively, ‘chase-your-tail’. An initial guess for the potential at the electrolyte boundary, $\phi_A(Q)$, is required to start the iteration process. Logical choices for $\phi_A(Q)$ include the potential ϕ_0 on the anode or the largest of the equilibrium potentials η_E . (The reader is reminded that only anode polarization is considered.) With this initial guess the boundary integral equations Eq. (9) can be solved to obtain the anode current density. The polarization equations, Eq. (5) and Eq. (6), provide a relationship between current and potential, which can be summarized as

$$\phi = \mathcal{F}(\mathcal{I}) , \quad (12)$$

and substituting this first current solution into this equation yields a new guess for the potential. In general, if ϕ^k denotes the potential at the k^{th} iteration step, \mathcal{I}^k the corresponding current solution obtained from the Laplace solution, then

$$\phi^{k+1} = \mathcal{F}(\mathcal{I}^k) , \quad (13)$$

and the process repeated until (hopefully) the change in potential is below a specified tolerance. This algorithm can be modified by including a relaxation factor β ,

$$\phi^{k+1} = (1 - \beta)\phi^k + \beta\mathcal{F}(\mathcal{I}^k) , \quad (14)$$

a measure of the trust one has that the new iterate is moving towards the solution.

The Picard iteration method is a completely general technique, and thus takes no account of the special aspects of the polarization and boundary element equations. Moreover, except for solving the Butler-Volmer equation (necessary to compute $\mathcal{F}(\mathcal{I})$), it does not solve a nonlinear equation at any step of the process. Although it has worked reasonably well for many electroforming situations, with both simple and complex geometries, these simulations involved only a single reaction and, probably most importantly, the physical parameters were such that the equations were only mildly nonlinear. For the multi-reaction electrospray analysis considered in [17] and herein, this simple method turned out to be very costly at best (slow convergence), and in some situations, failed to converge at all.

As an illustration of the unsuitability of this approach for electrospray analysis, Figure 1 displays the Picard convergence history for a simulation of a 2000μ length electrospray tube. (Complete details concerning the simulations will be presented in Section 5; here we simply wish to comment on the convergence difficulties.) The absolute value of the maximum change in potential is plotted versus iteration number, and the three curves represent different choices for the underrelaxation factor β . For $\beta = 10^{-2}$ there is no convergence, and in fact if the signed value were plotted, it would be seen to oscillate between plus/minus the value shown. For $\beta = 10^{-4}$, convergence appears to be possible, but clearly impractical regarding

computation time. Convergence is achieved for $\beta = 10^{-3}$, but in a very expensive 20000 iterations.

An attempt was made to accelerate the convergence of this algorithm by allowing the relaxation factor to be chosen adaptively during the course of the iteration. Depending upon the change in potential $\mathcal{F}(\mathcal{I}^k) - \phi^k$ over several steps of the iteration, β is adjusted appropriately: a larger value is chosen to speed convergence if no oscillation is detected, while a β is decreased if the iteration does not appear to be converging. While this strategy has been somewhat successful in reducing the time to convergence, the Picard approach nevertheless remains an expensive and not entirely trustworthy algorithm. The sensitivity of the convergence history to the value of β is clearly a serious problem for practical computations, as the range of values which achieve convergence is almost certainly problem dependent.

4 Polarization algorithm

There are a number of unappealing aspects of the fixed point approach, but the key problem appears to be in the cycling between the boundary integral Laplace solution, and the polarization relations. That is, in one iteration to the next, *all* values of potential (and in fact, all unknowns) are updated simultaneously. As a consequence, the iteration can oscillate between different ‘local’ solutions, and thus relaxation of the iteration is required to achieve convergence. Appropriate choice of this relaxation factor is almost certainly problem dependent, and as seen above, convergence, when achieved, can be exceedingly slow.

The additional concerns are, first, that as the current is computed from the Laplace equation, it is entirely possible to compute an unphysical value, *i.e.*, one that exceeds the limiting current \mathcal{I}_L . This causes obvious problems in trying to evaluate Eq. (6), and an *ad hoc* approach is required to come up with a reasonable η_{con} . Thus, for applications such as electrospray, wherein the concentration polarization can play a significant role, the fixed-point algorithm is likely to be less effective (in electroforming, current densities are in general well below the limiting current density). In addition, as will be discussed further below, the fixed point formulation becomes clumsy for the multiple reaction situation. The total current at a point is the sum of the currents for each reaction, and obtaining the individual currents from the total is not straightforward. Finally, just considering the numerics, the only nonlinear operation carried out in the fixed-point approach is the inversion of the Butler-Volmer equation to obtain η_{act} from the current. It seems reasonable to suppose that incorporating the solution of a nonlinear equation somewhere along the line would likely be beneficial for convergence.

The new algorithm described below seeks to correct these deficiencies, most especially the simultaneous updating of all potentials. It is convenient to first describe the algorithm for a single reaction. The extension to multiple reactions is quite straightforward and will only require a brief summary of the necessary modifications.

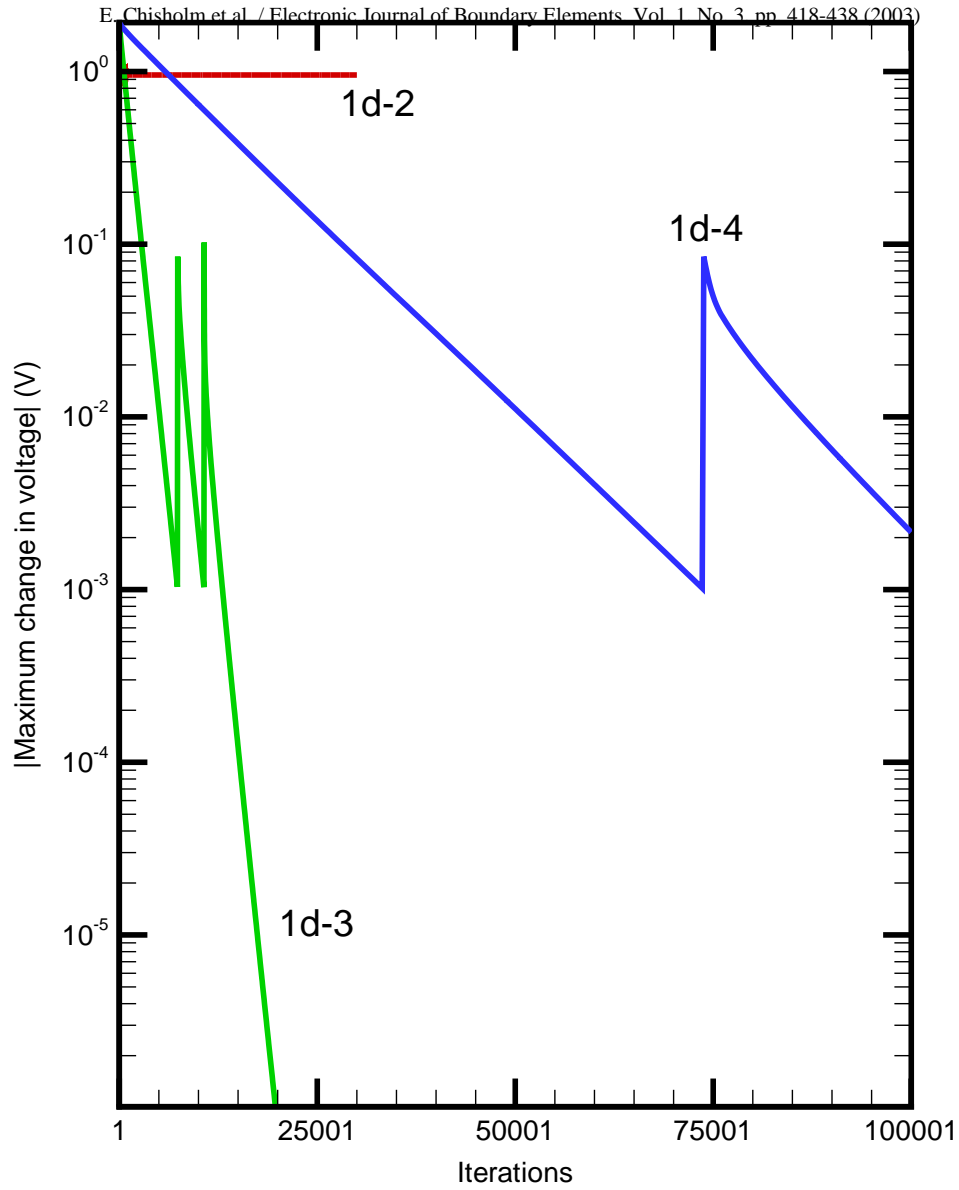


Figure 1: Convergence history for the Picard iteration for three relaxation factors. The emitter length is 2000μ .

4.1 Single Reaction

To describe the algorithm, we start with the boundary integral matrix equation Eq. (9), suitably rearranged. The anode nodes are collectively listed first, and the columns in H and G are swapped so that the anode currents are grouped together with the unknowns on the remainder of the boundary. This results in the linear system

$$\tilde{H} \begin{bmatrix} \phi^A \\ b \end{bmatrix} = \tilde{G} \begin{bmatrix} \mathcal{I}^A \\ x \end{bmatrix}, \tag{15}$$

where b denotes the known boundary data, x the unknowns on the non-anode part of the surface, and

$$\mathcal{I}^A = \begin{bmatrix} \mathcal{I}_1 \\ \vdots \\ \mathcal{I}_{M_A} \end{bmatrix} \quad \phi^A = \begin{bmatrix} \phi_1 \\ \vdots \\ \phi_{M_A} \end{bmatrix}, \tag{16}$$

are the vectors of anode currents and voltages (M_A being the number of anode nodes). Multiplying both sides by \tilde{G}^{-1} results in the block matrix system

$$\begin{bmatrix} \mathcal{I}^A \\ x \end{bmatrix} = \begin{bmatrix} A^{11} & A^{12} \\ A^{21} & A^{22} \end{bmatrix} \begin{bmatrix} \phi^A \\ b \end{bmatrix}, \tag{17}$$

where $A = \tilde{G}^{-1}\tilde{H}$. (Of course A is not computed in this fashion: the k^{th} column of A , A_k , is obtained by solving $\tilde{G}A_k = \tilde{H}_k$, the right hand side being the k^{th} column of \tilde{H} .) The rationale for reformulating the equations in this way is that it is now possible to write an equation for the current at anode node j

$$\mathcal{I}_j = \sum_k A_{jk}^{11} \phi_k + \sum_l A_{jl}^{12} b_l. \tag{18}$$

which does not involve any other anode current values. Moreover, as is well known, the boundary integral matrices are, roughly speaking, ‘local’, in that influences from nodes away from node j are relatively unimportant. This is a consequence of the Green’s function (Eq. (8)) dying off with distance. It is therefore likely that A will share this property, and this can be exploited by subtracting out the diagonal term in Eq. (18),

$$\mathcal{I}_j - A_{jj}^{11} \phi_j = \sum_{k \neq j} A_{jk}^{11} \phi_k + \sum_l A_{jl} b_l. \tag{19}$$

The potential ϕ_j can now be replaced by its equivalent in terms of current, Eq. (12),

$$\phi_j = \mathcal{F}(\mathcal{I}_j), \tag{20}$$

and we obtain

$$\mathcal{I}_j - A_{jj}^{11} \mathcal{F}(\mathcal{I}_j) = \sum_{k \neq j} A_{jk}^{11} \phi_k + \sum_l A_{jl} b_l. \tag{21}$$

The virtue of this form is that, treating all anode potentials except at node j as known quantities, this nonlinear equation can be solved for \mathcal{I}_j and ϕ_j . Cycling through the anode nodes, continually updating the right hand side with the new potentials, yields a Gauss-Seidel type iteration in which the latest information for ϕ^A is employed in solving the next nonlinear equation. A second benefit of the reformulation in Eq. (17) is that the iteration can proceed by dealing solely with the anode nodes: in the fixed-point algorithm, the solution for x is continually updated, which is costly and may contribute to the convergence problems. With Eq. (17), the solution for x (if needed) automatically falls into place once the values on the anode have converged.

Note that Eq. (21) is of the form $F(z) = 0$, and that there is some discretion in choosing what will play the role of the variable z . By opting to have z be the concentration polarization η_{con} , problems with the limiting current mentioned above, (*e.g.*, evaluating Eq. (6) with $\mathcal{I} \geq \mathcal{I}_L$) are avoided. Making this choice, the algorithm proceeds as follows:

1. For a value of η_{con} at the node under consideration, the current is obtained by inverting Eq. (6)

$$\mathcal{I} = \mathcal{I}_L \left(1 - e^{\frac{\eta_{con}}{RT}} \right) ; \quad (22)$$

2. Knowing the current, η_{act} is obtained from the Butler-Volmer equation, and then the total polarization is determined from Eq. (4);
3. Using a bisection algorithm, the value of η_{con} which satisfies Eq. (21) is determined, and the potential at this node is updated. An iteration step is the solution of Eq. (21), sweeping through all anode nodes;
4. The solution is considered converged when the maximum change in ϕ_j , $1 \leq j \leq M_A$, from one iteration to the next is less than a specified tolerance.

Regarding computational efficiency, the overhead in this algorithm can be reduced somewhat by making a few simple observations. First, the vector

$$\sum_l A_{jl}^{12} b_l . \quad (23)$$

that appears in Eq. (21) is obviously independent of the iteration, and is therefore computed once and saved. Second, the matrix-vector multiply

$$\sum_{k \neq j} A_{jk}^{11} \phi_k \quad (24)$$

is a large part of the total computation, and thus it is essential (for a FORTRAN implementation) to store the transpose of A instead of A . This allows accessing this matrix by columns. Also in this regard, employing the highly optimized BLAS [21] coding for this linear algebra operation is advantageous. Finally, when sweeping through the anode nodes to solve Eq. (21), it is not necessary to go through this

vector sequentially (*i.e.*, $j = 1$ to $j = M_A$). It has been found that convergence is faster if the list of anode nodes ordered by current, from the highest to the lowest current. This is intuitively reasonable, in that this will tend to cluster neighboring anodes. Moreover, the higher the current, the larger the polarization; thus, getting a reasonable estimate of these values helps speed convergence.

4.2 Multiple Reactions

As the application of the algorithm to more than two reactions is straightforward, it suffices to discuss the situation when two reactions are present. Fig. 2 schematically illustrates this situation. The two conditions which couple the separate polarization equations are first that the polarization for each reaction must yield the same effective anode potential [17]. Thus,

$$\phi_A = \eta_E^1 + \eta_{act}^1 + \eta_{con}^1 = \eta_E^2 + \eta_{act}^2 + \eta_{con}^2, \quad (25)$$

where the superscripts indicate the two different processes. Second, the total current at any point is the sum of the currents carried by individual reactions,

$$\mathcal{I} = \mathcal{I}^1 + \mathcal{I}^2. \quad (26)$$

To go from single to dual reactions only requires relatively minor modifications to the algorithm described in Section 4.1 above. Each reaction polarization is computed separately, beginning with the process having the largest equilibrium voltage, say reaction 1. As above, the controlling variable is chosen to be η_{con}^1 , and choosing a value for this quantity determines both the current for this reaction, and the anode potential ϕ_A . Knowing ϕ_A , Eq. (25) can be solved (again using the η_{con}^2 as the control variable) for the polarization and current for reaction 2. The total current input into Eq. (21) is then given by Eq. (26).

As mentioned above, figuring out how the current splits between the reactions is highly problematic for the fixed-point algorithm. In the present approach, this is handled automatically, and the ‘numerical interaction’ between the reactions is only through the relatively simple Eq. (25). Moreover, this approach clearly extends to more than two reactions.

5 Numerical Results

In this section, the polarization algorithm is applied in the study of electrochemical reactions inside an electrospray emitter tube. The emitter is employed in conjunction with a mass spectrometer and generates gas-phase ions from analyte species originally in solution, the gas eventually entering the spectrometer. The electrospray/mass spectrometry combination is an important tool which permits the analysis of a wide variety of analytes heretofore difficult or impossible to study using other techniques. Its applications span a broad range of categories, from simple molecular weight and structure determinations, to complex studies of the solution chemistries and gas-phase structures of biopolymers (see *e.g.*, [22, 23]).

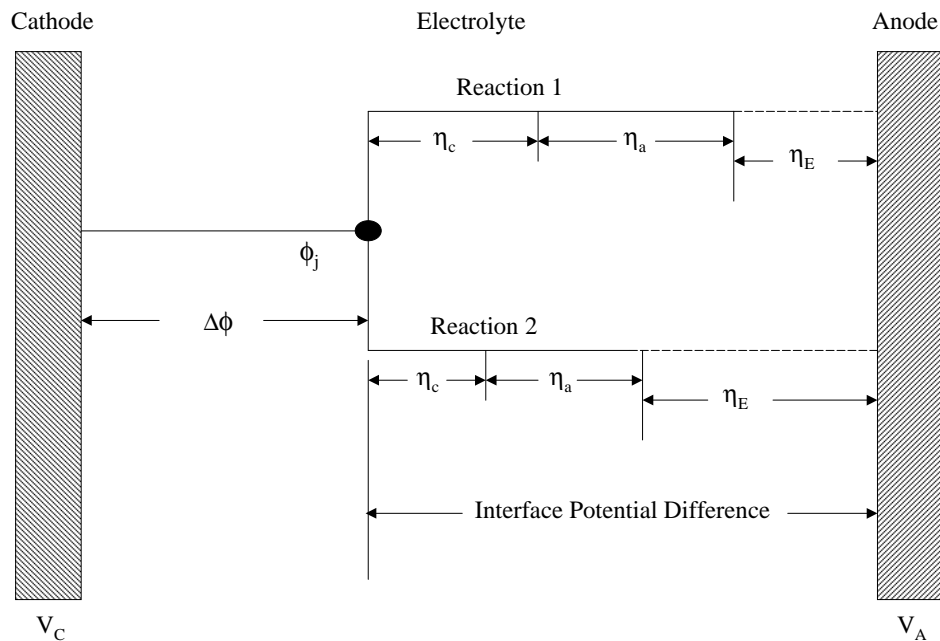


Figure 2: Schematic representation of two reactions at the anode surface.

The primary goal of the simulations is to understand the behavior of the electropray process as a function of the various parameters, and to help optimize these settings for specific applications. However, our goal herein is limited to demonstrating the performance of the new nonlinear iteration scheme. The physical model discussed below is sufficient and convenient for this purpose, but is not meant to be a completely faithful representation of the process.

A typical electropray ion source configuration, shown in Fig. 3, is comprised of two electrodes. The narrow-bore metal electropray emitter, held at a high voltage, and the atmospheric sampling aperture plate of the mass spectrometer, held at a voltage at or near ground. Under typical operating conditions, a solution containing the analyte of interest (which is normally ionic) is pumped through the emitter and sprayed towards the aperture plate. The spray is formed by the electrophoretic charge separation of ions in solution, which creates and charges the droplets. As presently understood, the charge-balancing process involves electrochemical oxidation/reduction of the components of the metal ES emitter and/or one or more of the species in the solution.

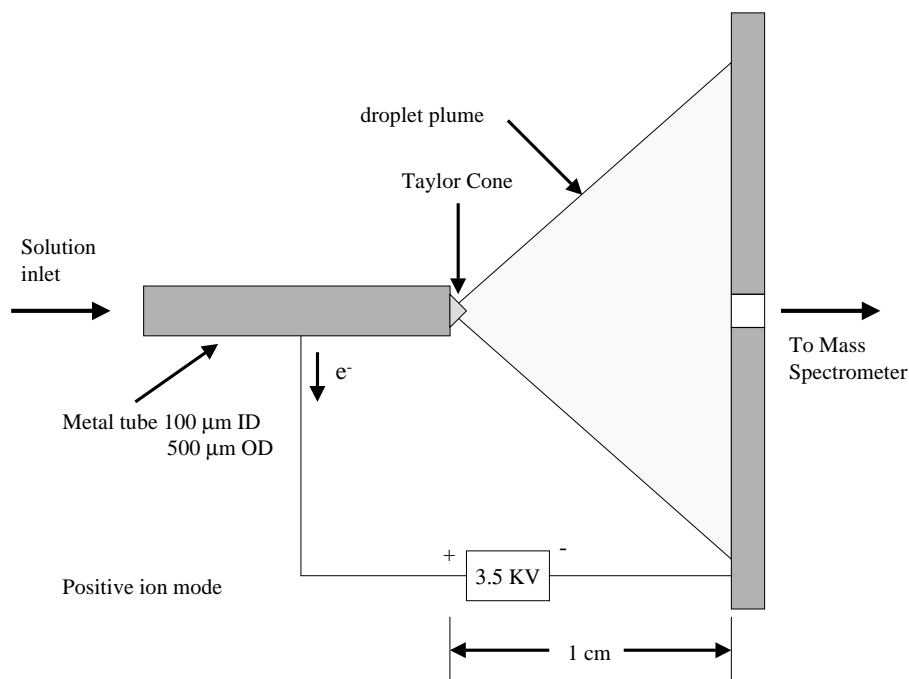


Figure 3: Electro spray mass spectrometry configuration.

The geometry employed in the boundary integral analysis of the emitter is shown in Fig. 4. The electrolyte solution was modeled as forming a truncated ‘Taylor cone’ (having a 49.3° angle at the base) at the emitter tip. The cone forms due to the balance between the electrical field forces and the surface tension of the liquid. For modeling simplicity, the actual cathode in Fig. 3 has been replaced by the flat virtual cathode (disk of radius 4.1μ held at a constant potential difference with respect to the anode of $\phi_C - \phi_A = -13V$) at the end of the Taylor cone. In this region, the isopotential surfaces are expected to be almost planar and, moreover, the virtual cathode is somewhat removed from the anode. Thus, this simplification is not expected to significantly affect the anode results. The side surface of the cone is modeled as an insulator (zero flux), and the anode is the cylindrical surface (radius 100μ) of the tube. The upstream end of the emitter has been capped off with an insulated surface, restricting the domain of the model to the region of significant electrochemical activity. Tables listing the various electrochemical parameters and other inputs to the simulation can be found in the Appendix.

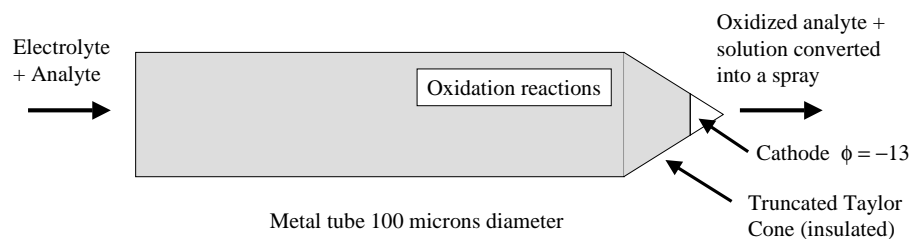


Figure 4: Geometry for the electro spray emitter tube simulation.

The most prominent redox reactions within the emitter under these conditions (further details and discussion about the chemistry can be found in [17]) are assumed to be H_2O oxidation,



and ferrocene oxidation,



In the following, we report results for three different length emitter tubes – 200μ , 400μ , and 600μ – and three different scenarios: water oxidation only, Fc oxidation only, and both reactions. In all cases, the tolerance for convergence of the anode potential was 3.0×10^{-5} . Table 1 shows the number of iterations to convergence for each tube length, and for the three chemistry models. Recall that in these calculations, the iteration through the anode went from highest to lowest current density. As an example of the improvement obtained, without this reordering the 600μ dual reaction calculation took 1009 iterations, roughly 4% slower. The convergence histories, for the three tube lengths, for the dual reaction calculation are shown in Fig. 5. In this graph, the logarithm of the maximum change in anode potential, from one iteration to the next, is plotted as a function of iteration number. The three curves refer to the length of the emitter tube.

Figure 6 presents a contour plot of the converged current density solution (both reactions) on the emitter tube. A uniform mesh was employed on the tube; however, the figure shows that the rapid variation in current is limited to the emitter end of the tube, and thus a finer mesh in this region would have been more appropriate. All three models (of differing lengths) used the same mesh

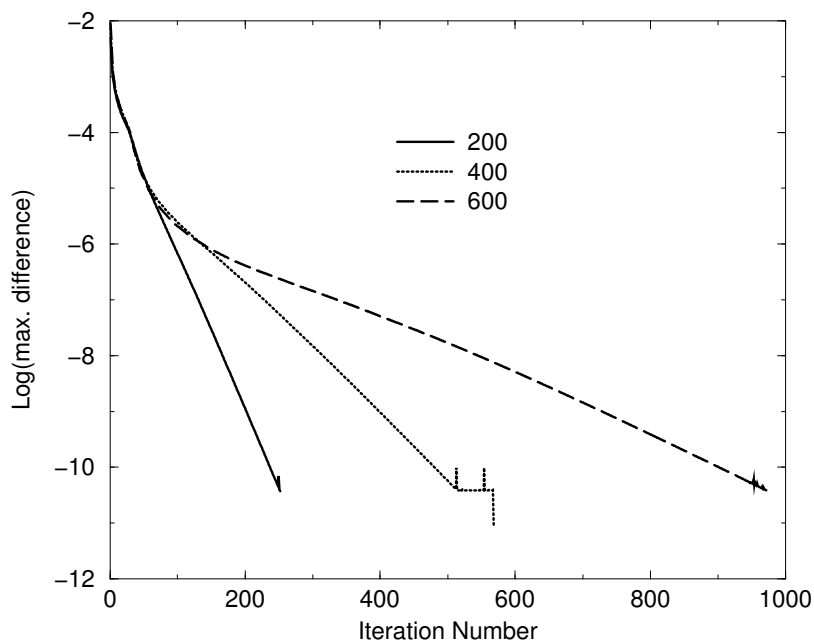


Figure 5: Convergence history for the dual reaction calculations.

(5033 nodes total, 3280 on the anode), the anode being scaled appropriately to achieve the appropriate size. Thus, the Laplace solution is less accurate for the larger lengths, resulting in the observed increase in the iterations required for convergence.

	200μ	400μ	600μ
Oxygen	253	525	972
Ferrocene	1694	3228	4922
Dual	252	515	972

Table 1: Number of iterations to convergence for electro spray analyses with different emitter lengths.

Note that the dual reaction converges in about the same number of iterations as the oxygen-only reaction, whereas ferrocene alone requires much more effort. This is due to the fact that the oxygen limiting current is appreciably larger than for ferrocene; thus, in the ferrocene-only calculation the currents are near to the

limiting value and are sensitive to small changes in potential. When the reactions are coupled, most of the current will go through the oxygen path, and thus the currents in each path will be sufficiently far from the limiting currents, and this does not play a significant role numerically.

It should also be noted that the large number of iterations required for ferrocene oxidation alone is not a cause for concern. This is an idealized condition which assumes that only this reaction is possible (e.g. no other species that can oxidize is present). Normally some other reaction will be able to carry some of the current and the ferrocene reaction would therefore assume a less significant role. The idealized condition forces the mathematical solution to drive the ferrocene reaction to the limiting current everywhere, a condition that takes many iterations to achieve a balance. The results for this case therefore model a situation that would be extremely difficult to achieve in practice, and therefore of little physical interest. It is presented here as an extreme test of the ability of the algorithm to converge. By comparison, the fixed point algorithm did not converge for this ferrocene only calculation.

As noted above, a key advantage of the new scheme compared to the Picard iteration is that an *ad hoc* relaxation factor is not required to achieve convergence. For the 2000μ length tube examined in Section 3, and a tolerance of 1.6×10^{-5} , the new algorithm converged in 277 iterations ($\kappa = 4.79 \times 10^{-10}$) and 736 iterations ($\kappa = 2.11 \times 10^{-9}$). In all of these simulations, both reactions are present. The corresponding convergence history (for the smaller conductivity) is shown in Fig. 7; the logarithm of the maximum change in potential over the tube (from one iteration to the next) is plotted versus iteration. Figure 8 plots the voltage and current solution (larger conductivity) in the near tip (axial distance = 1000, and $x = 1000$ is the emitter tip) region; in these simulations, the mesh was graded at the tip, and thus the current density solution is smoother than the uniform mesh solution shown in Figure 6.

6 Conclusions

Boundary integral methods provide a powerful tool for many types of electrochemical analysis [3, 4], and this paper addresses a key task in this modeling: the solution of the nonlinear polarization boundary conditions. An efficient ‘local’ Gauss-Seidel type iterative algorithm is obtained by inverting a boundary integral coefficient matrix to obtain the current as a function of the potentials. That the boundary integral formulation provides these direct equations relating surface current and potential, and hence makes possible this polarization algorithm, is another advantage to using this technique for electrochemical simulations.

Calculations involving one or two chemical reactions in an electrospray emitter tube have been carried out. A more complete discussion of the results of the simulations and a comparison with experimental data can be found in [24]. These calculations were shown to converge significantly faster than a ‘global’ Picard iteration in which all polarization values are updated simultaneously. Moreover,

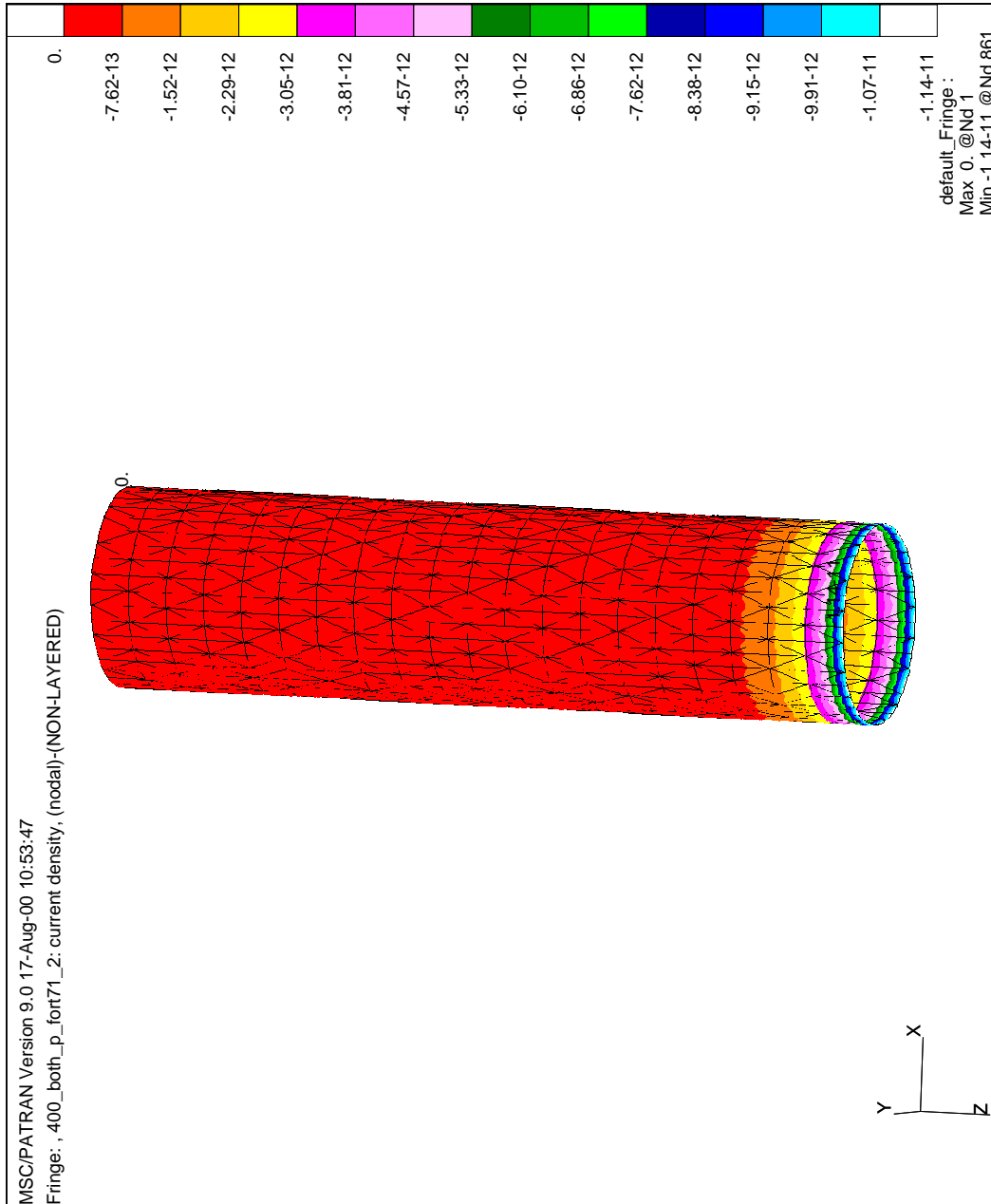


Figure 6: Converged solution (both reactions) on the emitter tube.

the Picard technique only converged if the iteration was relaxed, and then only for a limited range of values for the underrelaxation factor. The new algorithm does

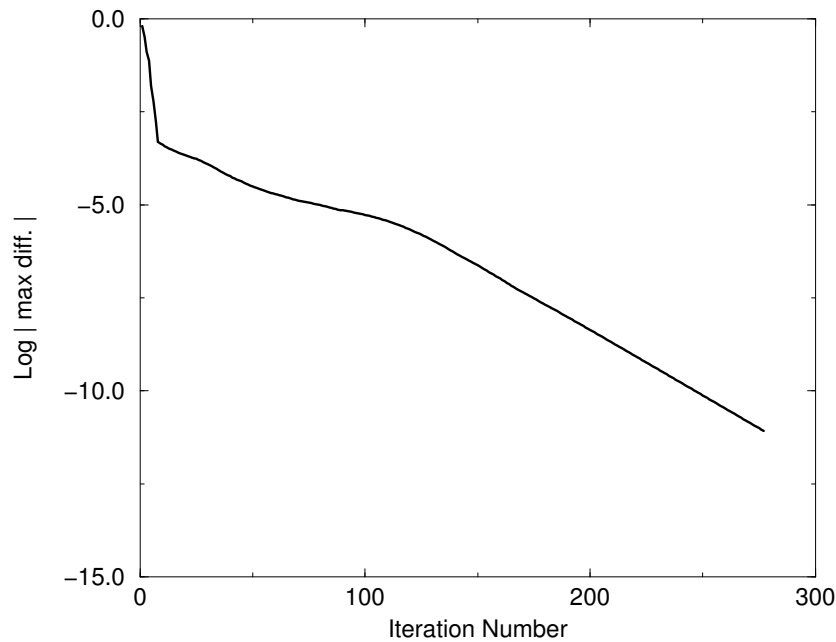


Figure 7: Convergence history, new algorithm, for a 2000μ emitter.

not employ relaxation factors.

Although the multi-reaction electrospray simulations reported herein are reasonably complicated, the geometry is nevertheless relatively simple. Further testing of this approach with more difficult geometries, such as occur in electroforming or Scanning Electrochemical Microscopy analyses, should be carried out. This work is presently being pursued.

Acknowledgment

This research was supported in part by the Applied Mathematical Sciences Research Program of the Office of Mathematical, Information, and Computational Sciences, U.S. Department of Energy under contract DE-AC05-00OR22725 with UT-Battelle, LLC. E. Chisholm acknowledges the support from the DOE Higher Education Research Experience (HERE) Program at Oak Ridge National Laboratory. The authors are grateful to J. Bullock for a critical reading of the paper and many valuable suggestions. They would also like to thank E. F. D'Azevedo, J. Bullock and G. Van Berkel for useful discussions.

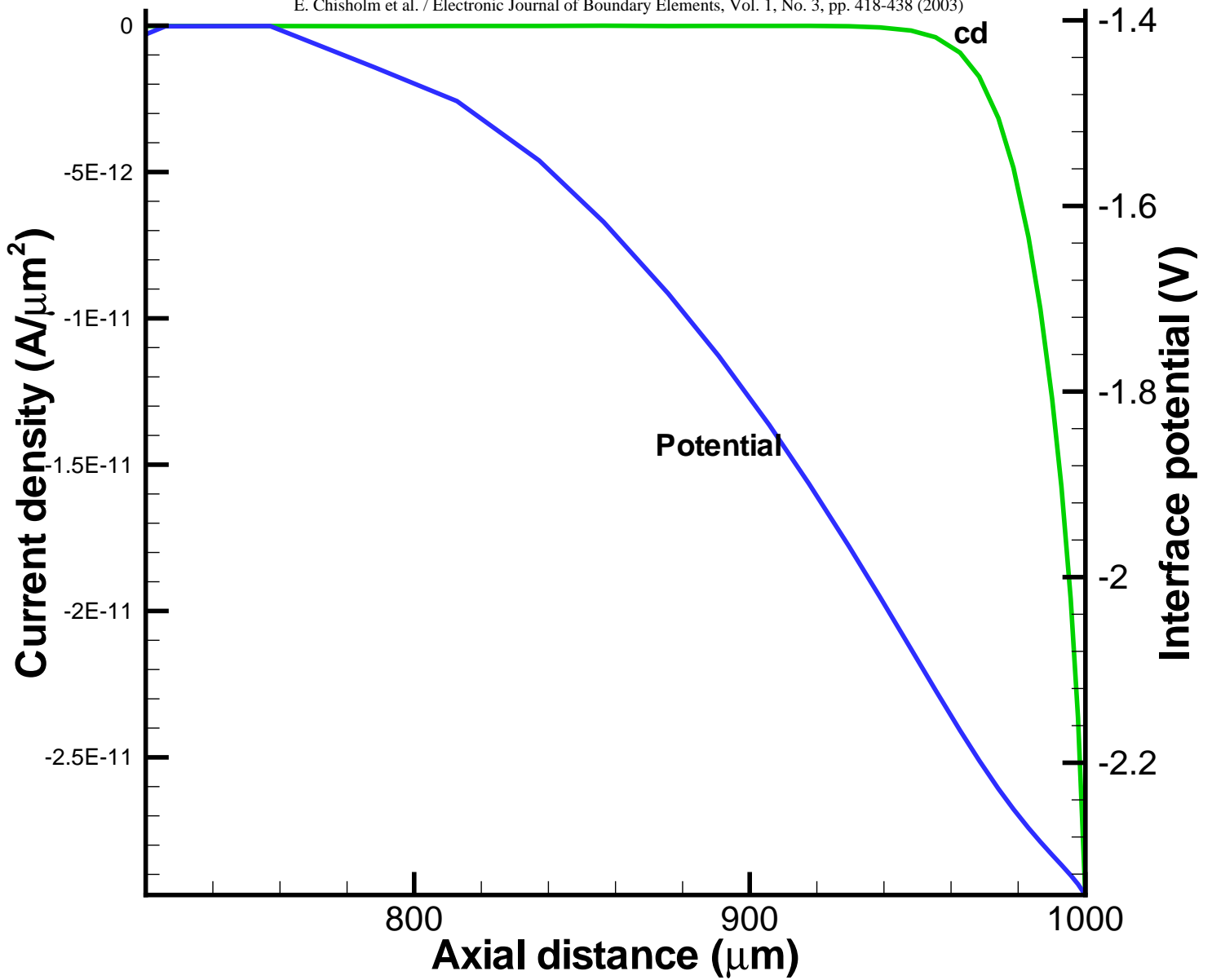


Figure 8: Near-tip converged polarization and current density solution for a 2000μ emitter.

References

- [1] M. Bonnet, Regularized direct and indirect symmetric variational BIE formulations for three-dimensional elasticity, *Engrg. Analy. Boundary Elem.*,

vol. 15, pp. 93–102, 1995.

- [2] C. A. Brebbia, J. C. F. Telles and L. C. Wrobel, *Boundary Element Techniques*, Springer-Verlag, Berlin and New York, 1984.
- [3] C. A. Brebbia (ed.), *Topics in boundary element research*, vol. 7, Springer Verlag, Berlin and New York, 1990.
- [4] Q. Fulian and A. C. Fisher, Computational electrochemistry: the boundary element method, *J. Phys. Chem. B*, vol. 102, pp. 9647–9652, 1998.
- [5] R. A. Adey and S. M. Niku, Computer modelling of corrosion using the boundary element method, in *Computer Modelling in Corrosion*, vol. ASTM STP 1154, pp. 248–269, American Society of Testing and Materials, Philadelphia, 1992.
- [6] S. Aoki and K. Kishimoto, Prediction of galvanic corrosion rates by the boundary element method, *Mathematical and Computer Modelling*, vol. 15(3-5), pp. 11–22, 1991.
- [7] V. G. DeGeorgi, A review of computational analyses of ship cathodic protection systems, in *BEM XIX*, pp. 829–838, Computational Mechanics, Southampton, 1997.
- [8] N. G. Zamani, J. F. Porter and A. A. Mufti, A survey of computational efforts in the field of corrosion engineering, *Int. J. Numer. Meth. Engrg.*, vol. 23(7), pp. 1295–1311, 1986.
- [9] J. S. Bullock, G. E. Giles and L. J. Gray, Simulation of an electrochemical plating process, in *Topics in boundary element research*, (ed.) C. A. Brebbia, vol. 7, chap. 7, pp. 121–141, Springer Verlag, Berlin and New York, 1990.
- [10] J. Deconinck, Electrochemical cell design, in *Topics in boundary element research*, (ed.) C. A. Brebbia, vol. 7, chap. 8, pp. 142–170, Springer Verlag, Berlin and New York, 1990.
- [11] G. E. Giles, L. J. Gray and J. S. Bullock, Validation of the BEPLATE code, in *1997 Electroforming Course and Symposium*, American Electroplaters and Surface Finishers Society, Orlando, FL, 1998.
- [12] Q. Fulian, A. C. Fisher and G. Denuault, Applications of the boundary element method in electrochemistry: scanning electrochemical microscopy, *J. Phys. Chem. B*, vol. 103, pp. 4387–4392, 1999.
- [13] Q. Fulian, A. C. Fisher and G. Denuault, Applications of the boundary element method in electrochemistry: scanning electrochemical microscopy, Part 2, *J. Phys. Chem. B*, vol. 103, pp. 4393–4398, 1999.
- [14] S. J. Badger, S. B. Lyon and S. Turgoose, Modeling the twin probe scanning electrode response, *J. Electrochemical Soc.*, vol. 145(12), pp. 4074–4081, 1998.

- [15] G. E. Giles, L. J. Gray, J. S. Bullock and G. J. V. Berkel, Numerical simulation of anodic reactions, in *Fundamental Aspects of Electrochemical Deposition and Dissolution Including Modeling*, (eds.) D. Landolt, M. Matlosz and Y. Sato, vol. PV 99-33, Electrochemical Society, New Jersey, 1999.
- [16] G. J. Van Berkel, The electrolytic nature of electrospray, in *Electrospray Ionization Mass Spectroscopy*, (ed.) R. B. Cole, chap. 2, pp. 65–105, John Wiley, New York, 1997.
- [17] G. J. Van Berkel, G. E. Giles, J. S. Bullock and L. J. Gray, Computational simulation of redox reactions within a metal electrospray emitter, *Analytical Chemistry*, vol. 71, pp. 5288–5296, 1999.
- [18] J. O. Bockris and A. K. N. Reddy, *Modern Electrochemistry*, Plenum Press, New York, 1970.
- [19] J. S. Newman, *Electrochemical Systems*, Prentice Hall, Englewood Cliffs, New Jersey, 1991.
- [20] M. Bonnet, *Boundary Integral Equation Methods for Solids and Fluids*, Wiley and Sons, England, 1995.
- [21] I. S. D. J. J. Dongarra, J. Du Croz and S. Hammarling, Algorithm 679: A set of level 3 basic linear algebra subprograms, *ACM Trans. Math. Soft.*, vol. 16, pp. 18–28, 1990.
- [22] R. B. Cole (ed.), *Electrospray Ionization Mass Spectroscopy*, John Wiley, New York, 1997.
- [23] S. J. Gaskell, *J. Mass Spectrom.*, vol. 32, pp. 677–688, 1999.
- [24] G. E. Giles, M. W. Wendell, G. J. Van Berkel, J. S. B. IV and L. J. Gray, Fluid dynamic and electrochemical simulations of a positive ion source electrospray emitter, in preparation.

Appendix: Parameters

The electrochemical parameters employed in the simulations are listed in the tables below.

Table 2: Polarization parameters.

Name	Symbol	Oxygen	Ferrocene	Units
Equilibrium half-cell potential	η_E	-1.229	-0.573	volts vs. H_2/H^+
Limiting Current	\mathcal{I}_L	$5.36E - 8$	$7.36E - 15$	$A\ cm^{-2}$
Exchange Current	\mathcal{I}_0	$1.00E - 20$	$2.17E - 12$	$A\ cm^{-2}$
Valence	n_V	2	1	moles electrons/mole
Transfer Coefficient	α_a	0.493	0.493	-
Transfer Coefficient	α_c	0.493	0.493	-

Table 3: Basic parameters.

Name	Symbol	Value	Units
Temperature	T	293.16	degrees Kelvin (K)
Cell voltage		-13.0	volts
Gas Constant	R	8.314	Joules K^{-1} mole $^{-1}$
Faraday Constant	F	96485	Coulomb/mole
Convergence tolerance		$1.6E - 5$	-